Geophysical Research Letters

Supporting Information for

Improving and harmonizing El Niño recharge indices

Takeshi Izumo[1,2] and Maxime Colin[3,4,5]

[1] Institut de Recherche pour le Développement (IRD), EIO laboratory, Université de la Polynésie Française (UPF), Tahiti, French Polynesia

[2] formerly at IRD, Sorbonne Université - CNRS-IRD-MNHN, LOCEAN Laboratory, IPSL, Paris, France

[3]Climate Change Research Centre, University of New South Wales, Sydney, New South Wales, Australia

[4]Laboratoire GEPASUD, University of French Polynesia, Tahiti, French Polynesia

[5]now at Leibniz Centre for Tropical Marine Research (ZMT), Bremen, Germany

Submitted to GRL on February 21st, 2022
Revised , August 2022

Contents of this file

Text S1 to S3; Tables S1 to S3; Figures S1 to S10

Introduction

The supplementary information contains 3 supplementary texts, 3 tables and 10 figures:

- Supplementary Text S1. *Data and methods*
- Supplementary Text S2. *Discussion on the mechanisms behind T_E and h_{ind} tendency equations*
- Supplementary Text S3. *Discussion on the choice of relative SST*

- Suppl. Table S1. Comparison of the r_{Te,h_ind} skill (using optimal h_{ind_eq+sw}) between various data and fields, filtering and ENSO indices.
- Suppl. Table S2. Regression coefficients robustness.
- Suppl. Table S3. 14-month lead hindcasts.

- Suppl. Fig. S1. Respective contributions of the r_{Te} skill and r_{h_ind} skill to the r_{Te,h_ind} skill.
- Suppl. Fig. S2. As one part of Fig. 2 but for ORAS5ext, 60-yr long period 1959-2018, comparing SLA, OHC and Z20.
- Suppl. Fig. S3. ENSO asymmetrical Ekman pumping.
- Suppl. Fig. S4. Regression maps of $h(x,y,t)$ or $h_{ind}(x,yt)$ onto $h(t)$ or $h_{ind}(t)$ indices.
- Suppl. Fig. S5. Harmonizing the various recharge indices by using h_{ind} index.
- Suppl. Fig. S6. Comparing a) ORAS5 SLA (with satellite SLA, and SLA, Z20 and OHC in ORAS5, for h_{ind_eq+sw} index (shown from 1993).
- Suppl. Fig. S7: as Fig. 3, but for satellite SLA over its shorter available period (1993-2021).
- Suppl. Fig. S8. As Fig. 3, but for ORAS5 Z20filt.
- Suppl. Fig. S9. Finding the best averaging box for h_{ind} to optimize both T_E and h_{ind} tendency equations of RO.
- Suppl. Fig. S10. Same as S9ab for ORAS5 SLAfilt (upper) and Z20filt (lower).

Supplementary Text S1. ***Data and methods***

Here we use classical monthly datasets : Optimum Interpolation SST OISSTv2 based on *in situ* observations and satellite measurements for the recent period (November 1981-Mar2022; Reynolds et al. 2002), HadiSSTv1.1 SST (1870-Mar2022; Rayner et al. 2003; similar results with SST from ECMWF ORAS5 oceanic reanalysis extended version over 1959-2018; Zuo et al. 2019) when using longer ORAS5 SLA/Z20, CMAP1 precipitation (from 1979; Xie and Arkin 1997), and windstress from the latest ECMWF ERA5 atmospheric reanalysis (from 1979 also; Hersbach et al. 2020; using former ERA-Interim reanalysis giving similar results; not shown).

We mostly use SLA as an accurate proxy of thermocline depth/OHC anomalies (e.g. Rebert et al. 1985; Gasparin and Roemmich 2017; Palanisamy et al. 2015), measured from satellites (1993-mid2021; Copernicus product), allowing a better and more homogeneous spatio-temporal sampling than the usual 20ºC isotherm depth Z20. We also verified that the results are robust with sensitivity tests shown in Supplementary Tables S1, S2 and S3 and Supplementary Figures S2, S6, S7, S8 and S10. Results are similar at 1st order with SLA, OHC and Z20 in ORAS5. For SLA, we subtract the 60°S-60°N global average at each time step to remove sea level rise global trend due to global warming, and we also remove any additional regional trend through a linear regression (results are similar without detrending).

For the ENSO index, T_E, we use the usual Niño3.4 region (170°W-120°W, 5°N-5°S), a reasonable compromise to capture central Pacific as well as eastern Pacific ENSO events (e.g. Takahashi et al. 2011, Capotondi et al. 2015; the present study focusses on typical ENSO events and neglect 2nd order spatial diversity). We define T_E as Niño3.4 relative SST (RSST, i.e. SST minus its 20°N-20°S tropical mean), as recommended by Izumo et al. (2020) and Van Oldenborgh et al. (2021) because atmospheric tropical deep convection interannual anomalies are rather related to RSST than to SST, notably in the presence of external forcing (see also Johnson and Kosaka 2016; Khodri et al. 2017; Izumo et al. 2018b; Williams and Patricola 2018, and Okumura 2019). The deep

convection threshold SST>~27-28°C (e.g. Gadgil et al. 1984) translates into RSST>~1°C, a threshold that remains valid with global warming (e.g. Johnson and Xie 2010). See Supplementary Text S3 for an extensive discussion justifying the relevance of RSST for RO equations.

T_E is normalized (divided by its standard deviation; STD), so that a 1-value represents typical ENSO amplitude. h is normalized when a regional average is done (e.g. usual 5°N-5°S, 120°E-80°W for h_{eq} and 5°N-5°S, 120°E-155°W for h_w), but not when taken at each (x,y) point, so that related regression maps represent typical anomalous amplitudes (cm for SLA, m for Z20). Using SST instead of RSST, or Nino3 instead of Nino3.4 region, makes T_E slightly less correlated to equatorial Pacific τ_x (i.e. ocean-atmosphere coupling), confirming that Nino3.4 RSST is a relevant choice. They anyway lead to very similar results, with slightly weaker skills when using Nino3 (Suppl. Table S2 and Suppl. Text S3).

Here we use typical statistical methods. The monthly seasonal cycle (computed by averaging each month of the year over the full period) is removed and intraseasonal variations are filtered out by a 4-month Hanning filter (3-point Hanning filter in pyferret software for monthly time series), so that periods lower than ~2-3 months are removed. For ORAS5 long analysis over its full period 1959-2018, we use in addition to the intraseasonnal low-pass filter a highpass Hanning filter (14-year window; i.e. 7 years cut on each side) to remove interdecadal variability with cutting frequency at ~10years (results are robust without this highpass filter, with just some increased interdecadal noise). Coefficients obtained from multivariate linear regression fits are shown multiplied by the STD of their multiplying variable (h or h_{ind}, cf. section 3), so as to represent typical amplitudes (STD(T_E) is already 1).

For statistical significance, we use Steigers Z-method for difference between two dependent correlations from a single sample (Hotelling William method giving similar results; https://www.quantitativeskills.com/sisa/statistics/correl.htm) and typical two-tailed Student t-tests for 90% confidence intervals. Using formulae (30) of Bretherton et al. (1999), we have about one effective degree of freedom every 4 months, i.e. ~85 for 1993-mid2021 (~140 for filtered ORAS5 data), a sufficiently large number leading usually to strong statistical significances of the results.

Here we explain how to obtain h_{ind_eq+sw} in details (and give the K dependance to data chosen for h) : 1) average over *eq+SW* box SLA (using $h(x,y,t) \sim SLA(x,y,t)$, detrended, smoothed, with seasonal cycle removed, cf. section 2) and then normalize, 2) remove its dependent part KT_E: $h_{ind\_eq+sw} = h_{eq+sw} - K_{eq+sw}\, T_E$, T_E being Niño3.4 relative SST anomaly (smoothed and normalized) with regression coefficient $K_{eq+sw} \approx 0.26[0.30/0.21]$ for satellite SLA[ORAS5_SLA/Z20] (K_{eq+sw} is conveniently already small thanks to *sw* addition to *eq* region, conversely to usual *eq* and *w* regions, for which $K_{eq} = +0.70[+0.68/+0.38]$ and $K_w = -0.40[-0.36/-0.51]$ respectively).

Supplementary Text S2. ***Discussion on the mechanisms behind T_E and h_{ind} tendency equations***

Here we explain physically and mathematically the spatial patterns of Fig. 2's various panels, very robust among datasets and periods (cf. Suppl. Fig. S2). And why there are similarities among some of them.

F_2 map shows us how $h_{ind}(x,y,t)$ would look like if ENSO windstress anomalies would blow for a long time, e.g. because of long-lasting La Niña conditions (mathematically because the temporal integral of dh_{ind}/dt equation (6) corresponds to the regression of h_{ind}(x,y,t) onto the temporal integral of T_E, as ε is negligible). The slow recharge in the western and central equatorial Pacific is consistent with former EOF analyses (e.g. Meinen and McPhaden 2000, Alory and Delcroix 2002, Clarke et al. 2007, Clarke 2010, Kumar and Hu 2014). As mentioned in the main manuscript, this western and equatorial recharge is through: 1) downwelling equatorial Rossby waves to the west (Wyrtki 1985, Jin 1997ab), and off-equatorial ones in the southwest; 2) upwelling equatorial Kelvin waves to the east forcing coastal Kelvin waves propagating poleward along the eastern boundary and thus a leakage of negative OHC anomalies towards the poles along the eastern boundary (Wyrtki 1985, Izumo et al. 2018a; vice versa for El Nino case). The recharge has also been suggested to be through Sverdrup transport towards the equator (Jin 1997a,b) but this is now debated (Clarke 2010; Zhu et al. 2018; Izumo et al. 2018a). Whatever the mechanisms, they are all formally well represented at 1st order by the term $-F_2T_E$.

Concerning the recharge meridional asymmetry with a larger recharge in the southwest, it is caused by Ekman pumping asymmetry, but not by the western boundary coastline meridional asymmetry, as mentioned in the main manuscript. This asymetrical Ekman pumping is mainly due south of ~7°S to windstress curl related to a poleward shift of the SPCZ (Suppl. Fig. S3). It forces locally downwelling (in the La Niña case) and thus slow off-equatorial downwelling Rossby waves progressively recharging the southwestern Pacific (see also Alory and Delcroix 2002; Cibot et al. 2005).

F_1 physically represents the slow recharge mode influence on T_E. F_1 tends to have a similar pattern to F_2, statistically because h_{ind} tends to co-vary in the west and southwest Pacific (as the spatial pattern of ENSO-related windstress remains at first order similar among ENSO events. Physically, the thermocline depth deepening related to a recharge (La Niña case) favors positive T_E through the thermocline feedback in the central Pacific (where coupling with convection is large; Clarke et al. 2007) and eastern Pacific (Wyrtki 1985, Jin 1997ab). Southwest and equatorial thermocline deepening can also increase transport-weighted temperatures T_{conv} and T_{EUC} of STCs (Shallow Subtropical/Tropical meridional overturning Cells) lower branches, and consequently T_E: the meridional pycnocline convergence T_{conv} (knowing that pycnocline convergence is larger in the southwest than in the northwest) and the equatorial undercurrent (EUC) T_{EUC}

(e.g. Izumo 2005, Ballester et al. 2015, 2016ab). As T_{conv} and T_{EUC} anomalies are at 1st order proportional to h (Izumo 2005), we would have these terms in the dT_E/dt equation:

$$f_{\_conv} * T_{conv} = f_{\_conv} * c * h_{\_eq+sw} = F_{1\_conv} * h_{\_eq+sw} = F_{1\_conv} * h_{ind\_eq+sw} + KF_{1\_conv} * T_E$$

$$f_{\_EUC} * T_{EUC} = f_{\_EUC} * c * h_{\_eq+sw} = F_{1\_EUC} * h_{\_eq+sw} = F_{1\_EUC} * h_{ind\_eq+sw} + KF_{1\_EUC} * T_E$$

So their influences on T_E can also be formalized as a term linearly proportional to h_{ind_eq+sw} plus one related to T_E. Thus they are implicitly included in the final term F_1.

The off-equatorial downwelling Rossby waves associated with the southwest Pacific recharge propagate to the western boundary coastal wave guide and then to the equatorial wave guide as Kelvin waves. They can also increase T_E through the thermocline feedback and STCs transport-weighted temperatures. Whatever the relative contributions of these mechanisms, their influences on T_E are implicitly included in F_1.

Supplementary Text S3. ***Discussion on the choice of relative SST***

Here we discuss the insensitivity of the results to our choice of using relative SST rather than usual SST. First of all, we have verified that the results are almost similar whatever the choice of SST or relative SST, with similar skill r_{Te,h_ind} (table S1): the skill differences are really weak, of ~0.01, not statistically significant at a high level, and much weaker than the skill improvement from former usual indices to h_{ind_eq+sw}.

If we go into details, there are some subtle 2nd order differences in the maps (not shown). For Nino3.4 SST, we have slightly less weight on central-eastern equatorial Pacific for dependent component (as compared to Fig. 1e), *i.e. the fast mode is not removed as efficiently, being essentially forced by equatorial Pacific τ_{x_eq}, which is more related to RSST through atmospheric deep convection.* Indeed, the correlation between T_E and τ_{x_eq} is 0.80 (i.e. explained variance of 64%) instead of 0.75 (57%) when using Nino3.4 RSST instead of Nino3.4 SST (and 0.75 (56%) instead of 0.71 (51%) for Nino3 region).

SST is theoretically the variable directly driven by the recharge process represented by the term $F_1 * h$ in the dT_E/dt equation. Yet, the recharge process is driven by windstress, which is itself directly driven by atmospheric deep convection and thus by RSST. Therefore, Nino3.4 RSST is better than usual SST for the term $F_2 * T_E$ in the *dh/dt* equation. Hence, theoretically, both choices could be considered.

Yet, in practice, RSST is what matters for ENSO global impacts through teleconnections and better captures coupled ocean-atmosphere anomalies related to ENSO (Okumura 2019; Izumo et al. 2020; Van Oldenborgh et al. 2021), especially with external forcing such as global warming (e.g. Vecchi and Soden 2008; Johnson and Xie 2010) or volcanic forcing (Khodri et al. 2016; Izumo et al. 2018b). Thus RSST is the variable we want to diagnose and possibly forecast seasonally. This is why we have chosen RSST.

r_{Te,h_ind} **skill** ***Comparing satellite/ORAS5***	**Sat. SLA (1993-2021)**	**Sat. SLA (1993-2018)**	**ORAS5 SLA (1993-2018)**	**ORAS5 Z20 (1993-2018)**	**ORAS5 OHC (1993-2018)**
from 1993	0.69	0.68	0.66	0.71	0.65
Comparing SLA/Z20/OHC in ORAS5	**SLAfilt**	**Z20filt**	**SLA**	**Z20**	**OHC**
from 1959	0.66	0.72	0.63	0.65	0.60
Testing ENSO indices	**Sat. SLA (1993-2021)**	**ORAS5 SLA**	**ORAS5 Z20**	**ORAS5 SLAfilt**	**ORAS5 Z20filt**
Nino3.4 RSST	0.69	0.64	0.67	0.66	0.72
Nino3.4 SST	0.70	0.65	0.66	0.68	0.72
Nino3.4 RSST	0.65	0.62	0.66	0.66	0.72
Nino3.4 RSST	0.66	0.63	0.65	0.64	0.72

Suppl. Table S1. Comparison of the r_{Te,h_ind} skill (using optimal h_{ind_eq+sw}) between various data and fields, filtering and ENSO indices. Upper rows: comparison between satellite and ORAS5 on the same period, from 1993. Central rows: skill stable over the long period 1959-2018 using ORAS5, with interdecadal variations filtered out ('*filt'*) or not. Bottom rows: verifying equivalence between ENSO indices. We have also verified the non-sensitivity to SST datasets: e.g. ORAS5 SST leads to almost no change (here we use OISST for recent periods and HadiSST for long periods from 1959).

Comparison for satellite SLA *(1993-2021)*	**R**	**F_1**	**F_2**	**ε**
h_w	0.06±0.04	0.15±0.04	0.15±0.04	0.06±0.04
h_{eq}	-0.18±0.05	0.25±0.05	0.25±0.05	-0.18±0.05
h_{eq+sw}	-0.05±0.03	0.18±0.03	0.18±0.04	-0.05±0.04
h_{ind_w}	0.00±0.04	0.13±0.04	0.13±0.04	0.00±0.04
h_{ind_eq}	0.00±0.04	0.16±0.04	0.17±0.04	0.00±0.04
h_{ind_eq+sw}	0.00±0.04	0.18±0.04	0.18±0.04	0.00±0.04
Comparison with ORAS5 *(for h_{ind_eq+sw})*				
ORAS5 SLA (1993-2018)	0.00±0.02	0.17±0.02	0.17±0.02	0.00±0.02
ORAS5 SLAfilt (1959-2018)	0.00±0.03	0.16±0.03	0.16±0.03	0.00±0.02
ORAS5 Z20filt (1959-2018)	0.00±0.03	0.16±0.03	0.16±0.02	0.00±0.02

Suppl. Table S2. **Regression coefficients robustness.** The sensitivity tests here show that, when using independent h_{ind} instead of usual h, values of the regression coefficients become stable for different recharge indices, data, fields (SLA and Z20) and periods: $F_1 \sim F_2 \sim 0.16$ to 0.18 ± 0.03, $R \sim \varepsilon \sim 0.0 \pm 0.03$ (for normalized indices, i.e. unit in month^{-1}).
Note that the RO, even if theoretically undamped as R and ε are negligible, is actually still damped because $residual_T$ (equation 6) is not a pure red noise but includes non-linear terms neglected in our 1st order linear approximation. Indeed, if we add to the T_E tendency equation a simple non-linear term cT_E^2 (quadratic term notably related to the non-linear response of convection to T_E; e.g. Jin et al. 2020; see An et al. 2020 review on more complicate possibilities, e.g. a multiplicative noise, see e.g. Jin et al. 2007, Graham et al. 2015, their equation (23)), the fit gives c=+0.05±0.03 and R= -0.01±0.03 month^{-1}. R becomes weakly negative (not at 90% level but robust for longer ORAS5 SLA and Z20; not shown), suggesting that the oscillator is weakly damped.

	r_{Te,h_ind} **skill**	**a (IOD)**	**b (h_{ind})**	**c (T_E)**
For satellite SLA (1993-2022):				
h_{ind_eq}	**0.50**	**-0.55**±0.36	**0.24**±0.28	**0.30**±0.36
h_{ind_eq+sw}	**0.58**	**-0.48**±0.34	**0.39**±0.26	**0.26**±0.34
For ORAS5 SLAfilt (1966-2011):				
h_{ind_eq}	**0.54**	**-0.50**±0.28	**0.32**±0.21	**0.10**±0.28
h_{ind_eq+sw}	**0.60**	**-0.43**±0.27	**0.42**±0.20	**0.05**±0.26
For ORAS5 Z20filt (1966-2011):				
h_{ind_eq}	**0.65**	**-0.43**±0.25	**0.48**±0.19	**0.05**±0.25
h_{ind_eq+sw}	**0.68**	**-0.40**±0.25	**0.52**±0.18	**0.03**±0.24

Suppl. Table S3. 14-month lead hindcasts. 14-month lead hindcasts of T_E in NDJ_{yr1} (November of year 1 to January of year 2) using ***a*IOD+b*h_ind+c*Te*** in SON_{yr0} (September to November of year 0), with coefficients *a, b*, *c* of the multivariate linear regression estimated from least-square fit.

Main messages of table S3 are:

1) adding the Southwest box (5ºS-15ºS, 120ºE-170ºW) improves the skill for all datasets/periods, more clearly for SLA than for Z20.
2) ORAS5 Z20 skill is better than ORAS5 SLA one, suggesting that thermocline depth metrics could perform better in a perfectly-observed ocean. Yet SLA has the advantage of being observed by satellite in near real-time, and the additional advantage of being more available in climate models outputs (e.g. CMIP) than Z20.
3) we have statistically-significant contributions from h_{ind_eq+sw} and IOD, but not from T_E itself (the IOD contribution *a* is always significantly negative, while the coefficient *c* for ENSO itself is never significant at 90% level). Hence this improved recharge index with updated datasets confirms earlier studies emphasizing the IOD influence on following year's ENSO phase (Izumo et al. 2010, 2014, 2016, Dayan et al. 2014, Jourdain et al. 2016). Regression coefficients have qualitatively similar values among datasets/periods.

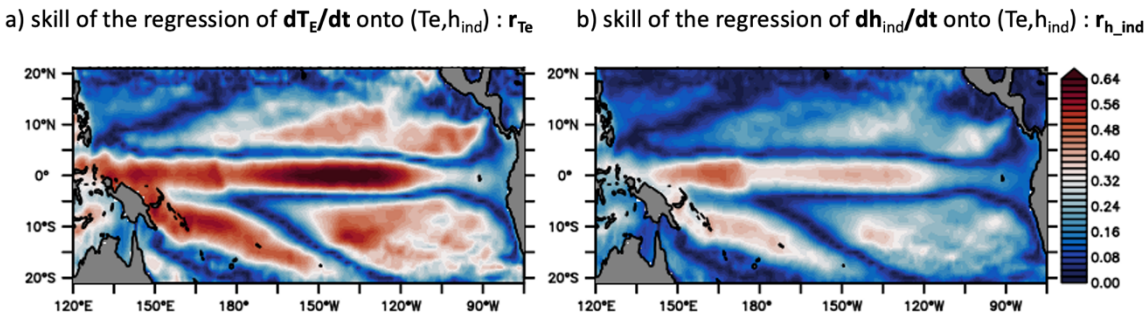

Suppl. Fig. S1. Respective contributions of the r_{Te} skill and r_{h_ind} skill to the r_{Te,h_ind} skill. a) correlation skill r_{Te} for the regression of dT_E/dt onto $(Te(t),h_{ind}(x,y,t))$ (equation 4). b) same but for r_{h_ind} for the regression of dh_{ind}/dt. They both contribute to the skill r_{Te,h_ind} shown in Fig. 2k for the tendency equation of the vector (Te,h_{ind}), since we can show that $r_{Te,h\_ind}^2 \approx (r_{Te}^2 + r_{h\_ind}^2)/2$ for normalized vectors, as T_E and h_{ind} are by definition uncorrelated, and as their tendencies are also almost uncorrelated (<0.1). Note that r_{Te} tends to have a similar spatial pattern to r_{h_ind}, but of stronger amplitude (though with also relatively larger central-equatorial values). The similarity of the spatial patterns, notably with the strong skill in the west and southwest Pacific, is likely because h_{ind} tends to vary in phase in the west-central equatorial Pacific and southwest tropical Pacific (cf. Supplementary Text S2). r_{Te} tends to be of larger amplitude than r_{h_ind}, partly because $dT_E(t)/dt$ is less noisy (T_E being a box average) than $dh_{ind}(x,y,t)/dt$, which is for each (x,y) point. The pair $(Te(t),h_{ind}(x,y,t))$ can thus more easily explain $dT_E(t)/dt$ variance than dh_{ind}/dt variance.

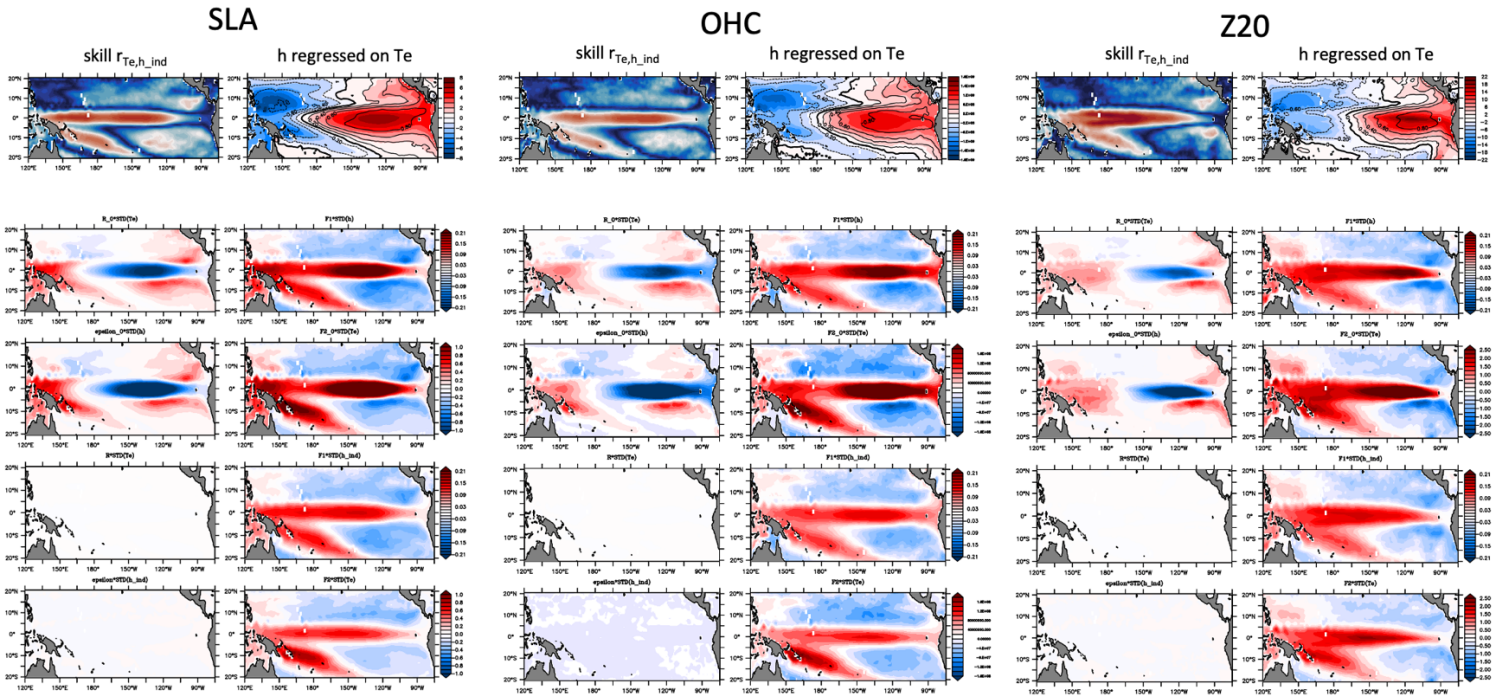

Suppl. Fig. S2. Equivalent (partly) **to Fig. 2** (based on 1993-2021 satellite SLA) **but for ORAS5 (60-yr long period 1959-2018), comparing SLA** (left)**, OHC** (middle) **and Z20** (right)**.** First upper-left panel is the skill map, as Fig. 2k. 2nd upper panel is the regression of h onto T_E (the fast mode), as Fig. 1b. Panels of 2nd and 3rd row panels are for usual non-orthogonal (T_E,h) basis, as Fig. 2a,b,e,f. Panels of 4th and 5th rows are for orthogonal (T_E,h_{ind}) basis, as Fig. 2c,d,g,h. SLA is as in Fig. 2 in cm. OHC is the oceanic heat content from ocean surface to bottom in J. Z20 is the 20ºC isotherm depth in m.

Main messages of figure S2 are:

1) ORAS5 SLA gives similar results to satellite SLA (we have also tested the sensitivity to the periods chosen: ORAS5-based maps are similar for 1959-2018 and shorter 1993-2018 period).
2) SLA, OHC and Z20 are qualitatively similar, with some differences in patterns and in the correlation between T_E and h. OHC spatial patterns tend to be in between SLA and Z20 patterns, but the skill is weaker. Note that lag-0 correlation with T_E is weaker for Z20 than for SLA, possibly because of 1st baroclinic mode playing more role for Z20 than for SLA, which will be more influenced by higher modes, notably the 2nd baroclinic mode (not shown). These different baroclinic mode contributions could partly explain some differences in results between Izumo et al. (2018a) study, based on the LCS model that take into account several baroclinic modes, and Neske and McGregor (2018) study based on a shallow water model, which only simulates the 1st baroclinic mode.

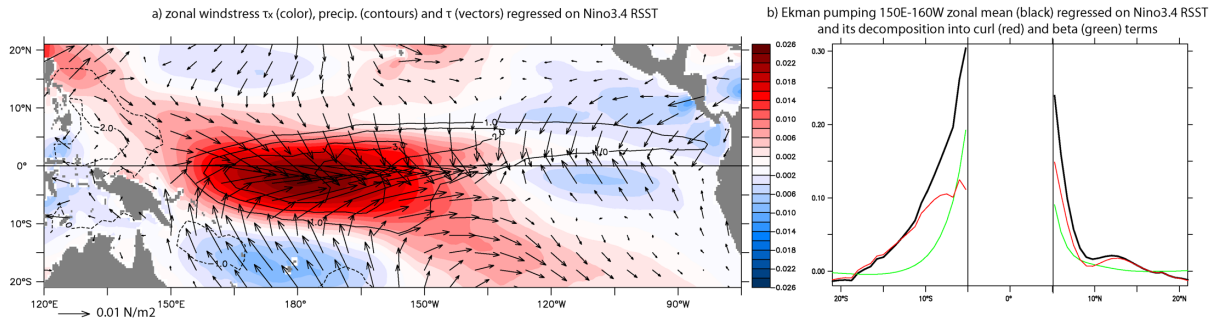

Suppl. Fig. S3. ENSO asymmetrical Ekman pumping. a) Zonal wind stress τ_x (color, N.m^{-2}), precipitation (contours, mm.day^{-1}) and wind stress τ (vectors) regressed on T_E. **b)** Regression of the 150°E-140°W zonal mean of Ekman pumping (black, 10^{-5}m/s) on T_E, and Ekman pumping decomposition into its wind stress curl (red) and beta τ_x (green) terms, only defined out of the 5°N-5°S equatorial band (shown by vertical lines).

In the southern hemisphere, the decomposition shows that south of ~7°S, the wind stress curl term is the main contributor to Ekman pumping, while north of ~7°S, the beta term is also important. Hence, Ekman pumping asymmetry is mainly due to wind stress curl (curl itself mostly due to -$d\tau_x/dy$; not shown), with some added asymmetry from beta τ_x term (Yokoi et al. 2008), large between ~7°S and 5°S.

Note that the western boundary coastline meridional asymmetry would conversely favor a larger northwest recharge, as shown by an LCS (Linear Continuously Stratified model; McCreary 1980) idealized experiment with a symmetric zonal wind stress forcing (Izumo et al. 2018, their Fig. 5). We have done a similar experiment, but with a more realistic ENSO-like asymmetric windstress (with easterlies shifted to the south during La Niña, plus a reversal to westerlies at ~15°S, related to a poleward shift of the SPCZ (*vice versa* for El Niño case, cf. Suppl. Fig. S3a; see also Alory and Delcroix 2002; Cibot et al. 2005; McGregor et al. 2013). This asymmetry indeed favours a larger southwest recharge (not shown).

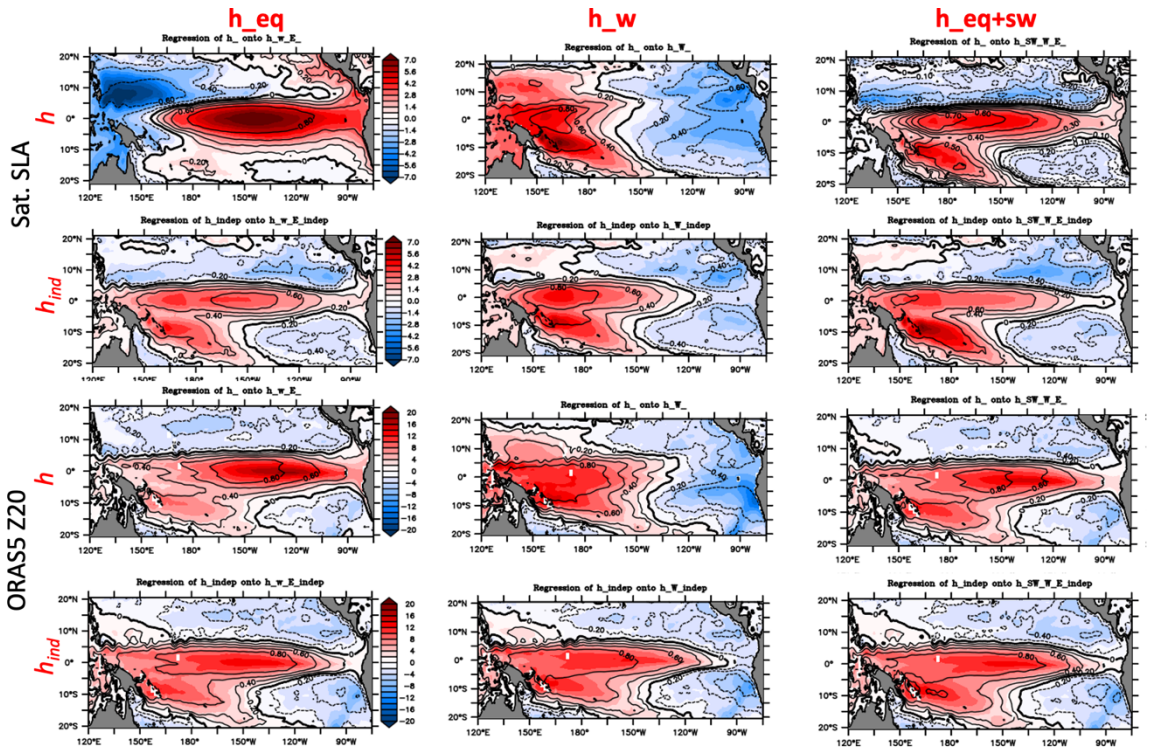

Suppl. Fig. S4. Regression maps of *h(x,y,t)* or $h_{ind}(x,yt)$ onto *h(t)* or $h_{ind}(t)$ indices. Spatial patterns associated with h_{eq} (left column), h_W (middle column) and h_{eq+sw} (right column) look significantly closer for h_{ind} (2nd and 4th rows) than for usual full h (1st and 3rd rows). I.e. h_{ind} harmonizes recharge metrics, making indices converge. First two rows are based on satellite SLA, the last two on ORAS5 Z20filt.

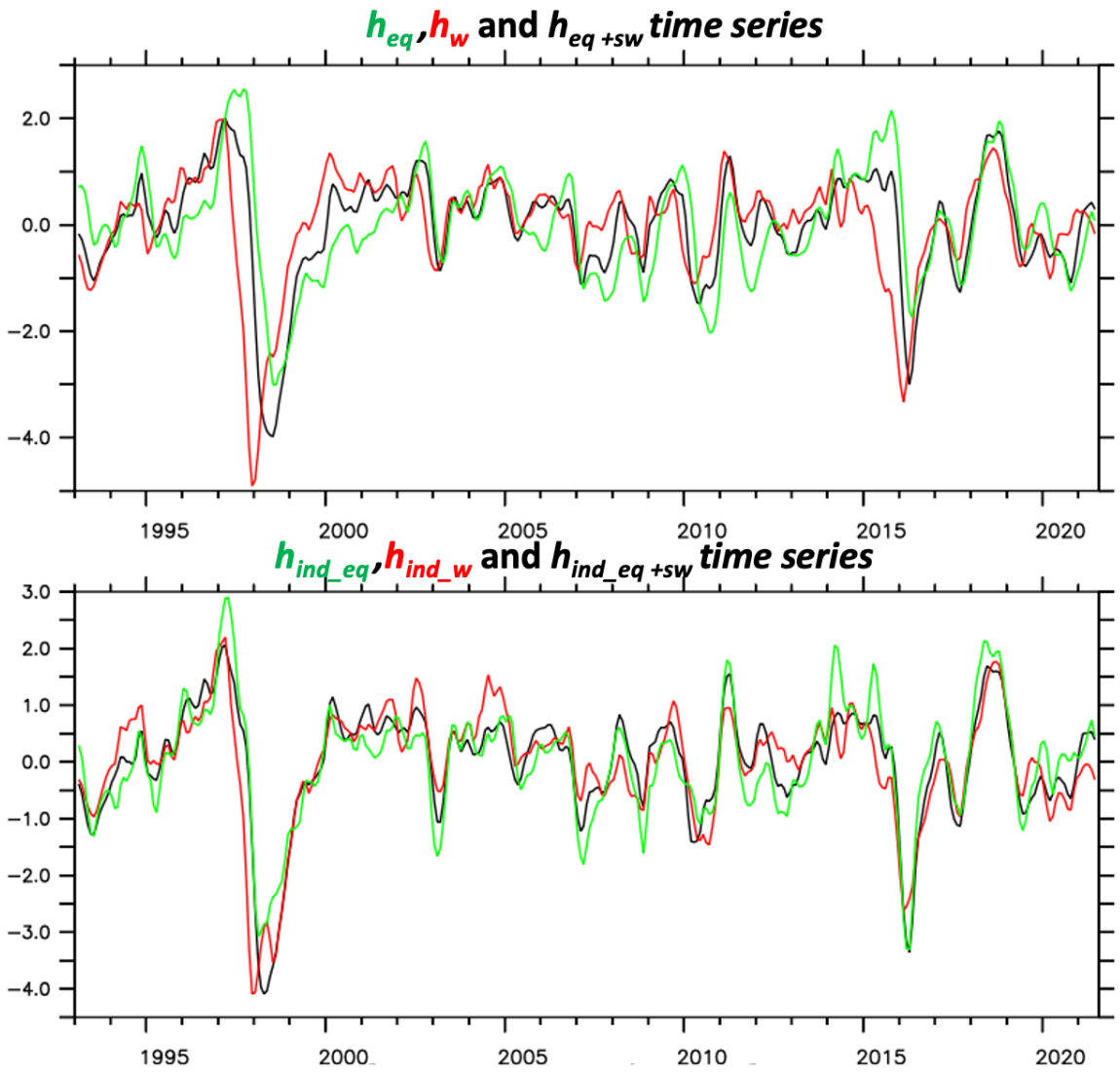

Suppl. Fig. S5. Harmonizing the various recharge indices by using h_{ind}. Indices are much better correlated for independent component than for full signal:
r(h_{ind_eq},h_{ind_w})= 0.79 (r^2=62%) instead of 0.18 (3%)
r(h_{ind_eq},h_{ind_eq+sw})= 0.91 (82%) instead of 0.79 (62%)
r(h_{ind_w},h_{ind_eq+sw})= 0.88 (78%) instead of 0.67 (44%)
This confirms that using h_{ind}, i.e. removing the dependent component, helps in reconciliating and harmonizing the various recharge indices used in the literature. Furthermore, h_{ind_eq+sw} is close both to h_{ind_eq} and h_{ind_w} (results shown here for satellite SLA).

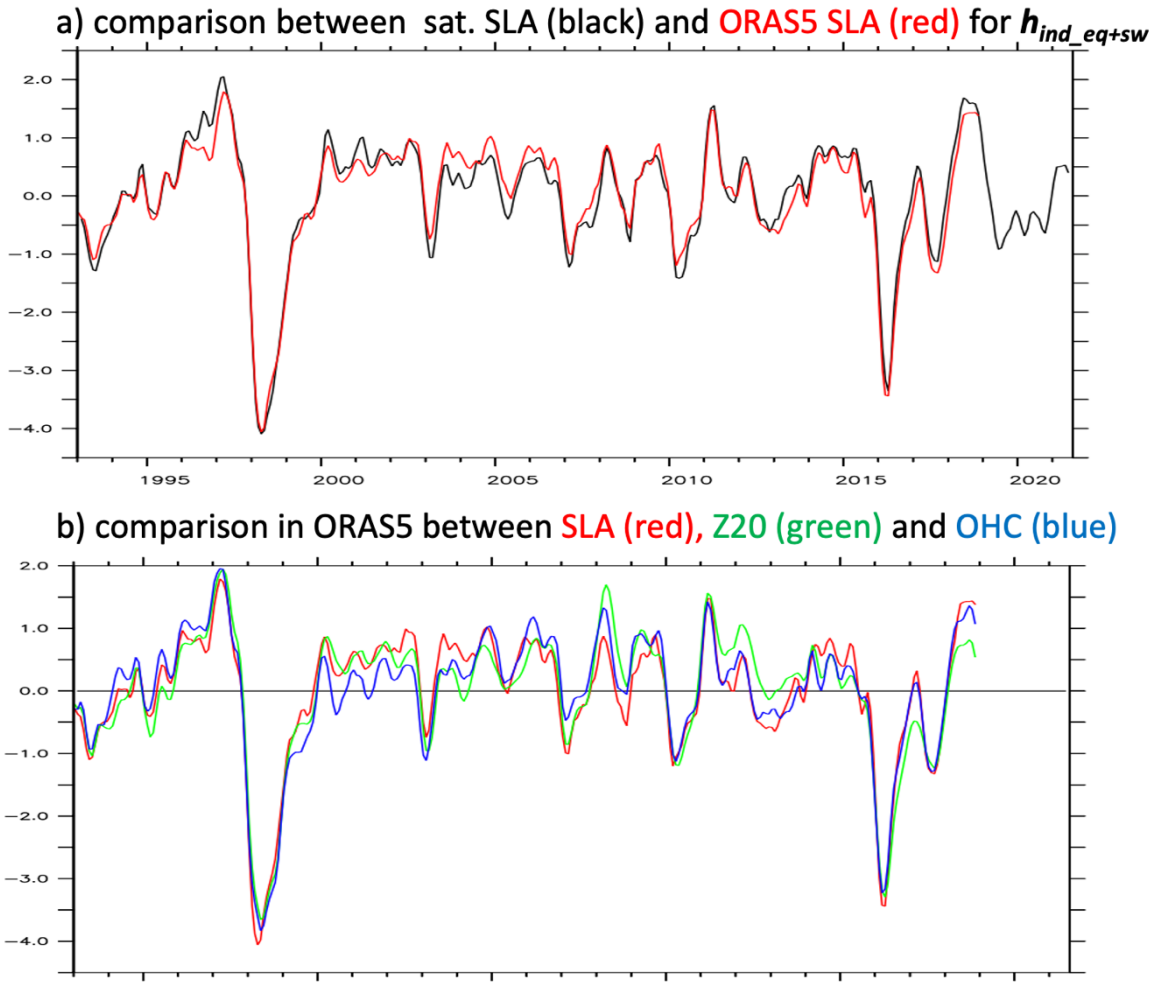

Suppl. Fig. S6. Comparing a) ORAS5 SLA (red) **with satellite SLA** (black), **and b) SLA** (red), **Z20** (green) **and OHC** (blue) **in ORAS5** (lower)**, for h_{ind_eq+sw} index (shown from 1993).** Panel a validates ORAS5 SLA, highly correlated (r=0.97; r^2=*95%*) to observed satellite SLA for h_{ind_eq+sw} (and also for h_{ind_eq} and h_{ind_w}; not shown; ORAS5 shown here without high-pass decadal filter here for comparison with satellite SLA; note that ORAS5 may not be as good before 1993 before which the reanalysis does not assimilate satellite sea level observations). Panel b shows that, in ORAS5, SLA is highly correlated to Z20 (r=0.94; r^2=*88%*) and OHC (r=0.96; r^2=*92%*), i.e. SLA, Z20 and OHC are almost equivalent for h_{ind_eq+sw} (and also for h_{ind_eq} and h_{ind_w} ; not shown).
Note that using h_{ind} instead of full h also harmonizes SLA-based and Z20-based metrics: e.g. the squared correlation between SLA-based h_{eq} and Z20-based h_{eq} is r^2=81% (88%) instead of 72% (81%). Adding the Southwest further increases r^2 to 85% (0.90) for full h_{eq+sw} and even to 88% (0.92%) for independent h_{ind_eq+sw}. The r^2 value is given over the 1993-2019 period (in parenthesis if whole ORAS5 period with decadal filter applied).

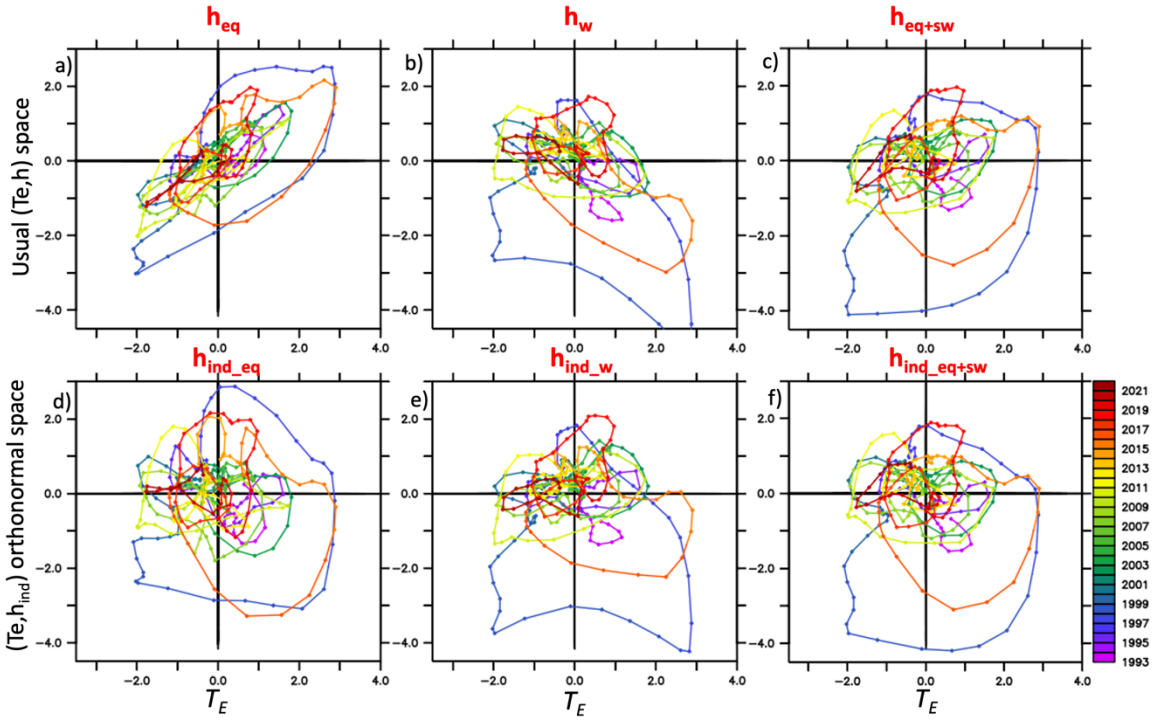

Suppl. Fig. S7: as Fig. 3, but for satellite SLA over its shorter available period (1993-2021).

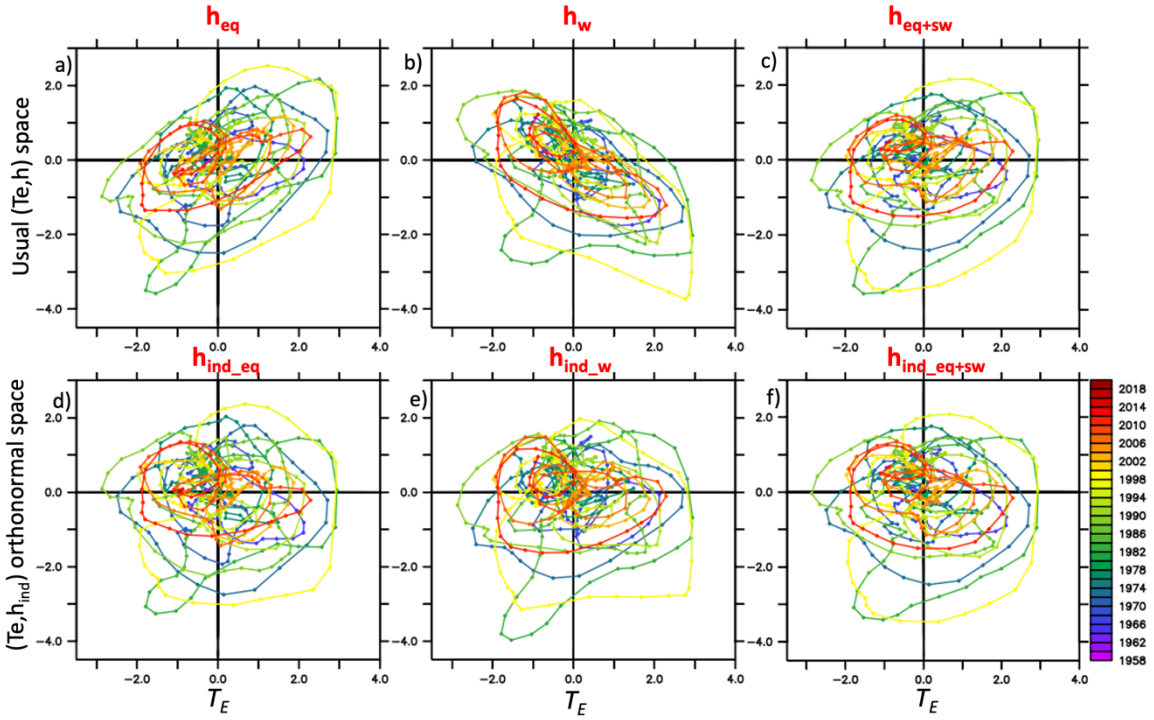

Suppl. Fig. S8. As Fig. 3, but for ORAS5 Z20filt. Results are robust, with only 2nd order differences. E.g. extreme El Niño events cause a weaker discharge in Z20 than in SLA (and thus a weaker El Niño/La Niña asymmetry). Hence, bottom panels look even more circular and closer to ideal RO trajectories when using Z20 instead of SLA (and when removing decadal variability, done here).

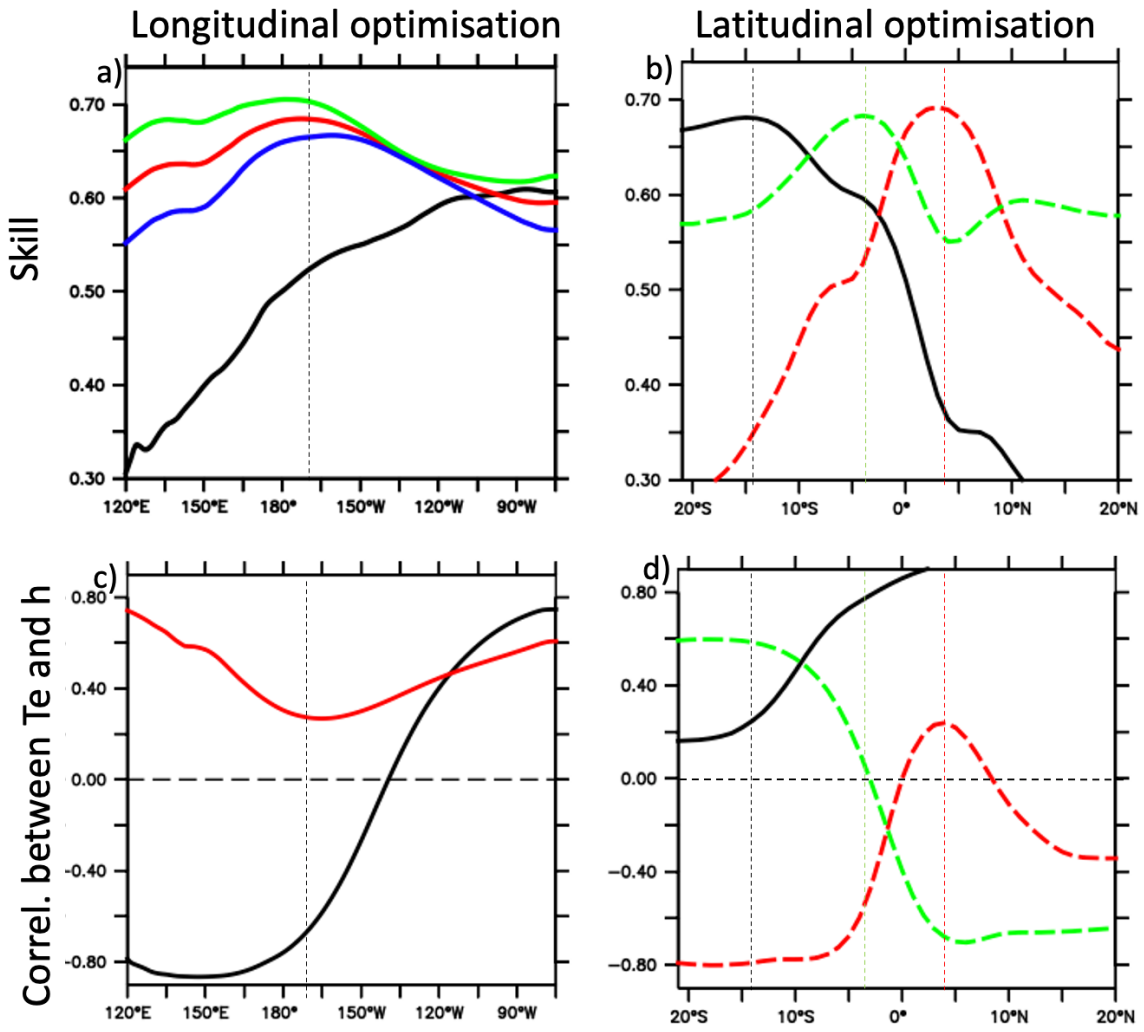

Suppl. Fig. S9. Finding the best averaging box for h_{ind} to optimize both T_E and h_{ind} tendency equations of RO. Panel a is almost similar to Fig. 2j, showing the optimization of the eastern edge longitude. The black line shows the skill r_{Te,h_ind} for h_{ind} averaged over: the equatorial band (5°N-5°S) with its western edge fixed to 120°E and its eastern edge varying, given by the x-axis. The black line shows that the optimal eastern edge for the equatorial band is at equatorial Pacific eastern boundary, 80ºW. Red line is for a two-rectangle region, this classical equatorial box (5°N-5°S, 120°E-80°W) plus a southern 5°S-15°S box with the same western edge fixed at 120°E and its eastern edge varying. Its optimal is around 170ºW (indicated by a dashed black vertical line, i.e. *eq+sw* region). The green and blue lines are similar to the red line, but specifically for r_{Te} and for r_{h_ind} respectively. **Panel c** shows the associated lag-0 correlation between T_E and h, for the same regions as the black and red lines in panel a. The lag-0 correlation interestingly is almost the lowest for the optimal *eq+sw* region. This is an additional interest of this region, e.g. the difference between h_{ind_eq+sw} and h_{eq+sw} is much weaker than between h_{ind_eq} and h_{eq}. Concerning the western edge longitude, the optimal is around 100ºE-120ºE, so we have kept 120ºE to stay in Pacific, as Meinen and McPhaden (2000) choice. **Right panels** are showing the optimization of the latitudinal edges of the h_{ind} two-rectangle averaging region. The black line is for the southern edge of the southwest rectangle (120ºE-170ºW, 5ºS to y_{sw} indicated in horizontal axis, the other region being fixed to the classical equatorial box 5°N-5°S, 120°E-80°W). y_{sw} optimum is around 16-12ºS (cf. black dashed vertical line at 14ºS), confirming that 15ºS is a good simple choice. The green line is for the southern edge of the equatorial band rectangle (120°E-80°W; 5ºN-y_{eqS}, the southwest region

being 120ºE-170ºW, 15ºS to y_{eqS}). The optimum is around 6-2ºS, confirming that 5ºS is a good simple choice. The red line is for equatorial band northern edge (120°E-80°W; 5ºS-y_{eqN}, the southwest region being 120ºE-170ºW, 15ºS to 5ºS). The optimum is around 2-6ºN, confirming that 5ºN is a good simple choice. Note that theoretically, we could even do a multivariate optimization. We have done some tests that confirm our choice (e.g. if y_{sw}=14°S, y_{eqS}=4°S and y_{eqN}=3°N, skill is 0.70, only slightly larger than 0.69 for 15°S, 5°S,5°N, both skills being much higher than 0.61 for classical h_{eq}), within the range of uncertainties (e.g. differences between satellite SLA shown here and ORAS5 Z20filt in next figure). All these analyses confirm that the optimal, and still simple, region combines the classical equatorial band (5ºS-5ºN, 120ºE-80ºW) and the southern band 15ºS-5ºS, from 120ºE to about 170ºW, i.e. $h_{ind\ eq+sw}$.

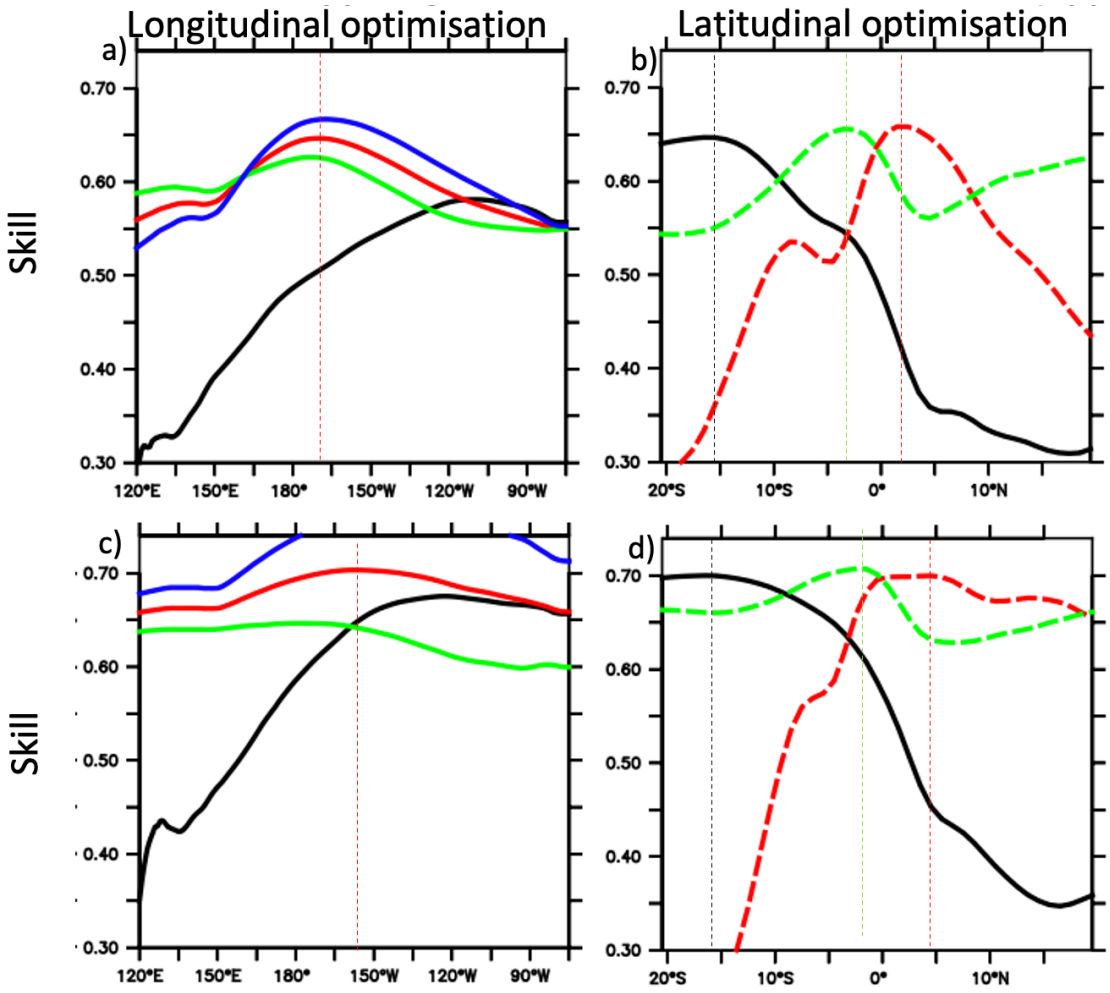

Suppl. Fig. S10. Same as S9ab (based on satellite SLA) **but using ORAS5 SLAfilt (upper) or ORAS5 Z20filt (lower).** Upper panels show that ORAS5 SLA results are consistent with satellite ones, with similar optimal longitude and latitudes (skill overall slightly weaker). Lower panels show that Z20 is overall consistent with SLA, with however less sharp latitudinal edges and an optimal eastern edge of southwest rectangle at ~155ºW instead of ~170ºW. But the difference between these two longitude choices is *in fine* not significant anyway (almost similar skill, and correlation of 0.99 between the two definitions). Therefore, SLA and Z20 are almost similar for h_{ind_eq+sw} (correlation of 0.96, cf. Fig. S6b).